

Mutations in *GPR143/OA1* and *ABCA4* Inform Interpretations of Short-Wavelength and Near-Infrared Fundus Autofluorescence

Maarjaliis Paavo,¹ Jin Zhao,¹ Hye Jin Kim,¹ Winston Lee,¹ Jana Zernant,¹ Carolyn Cai,¹ Rando Allikmets,^{1,2} Stephen H. Tsang,^{1,2} and Janet R. Sparrow^{1,2}

¹Department of Ophthalmology, Columbia University Medical Center, New York, New York, United States

²Department of Pathology and Cell Biology, Columbia University Medical Center, New York, New York, United States

Correspondence: Janet R. Sparrow, Department of Ophthalmology, Columbia University Medical Center, 635 W. 165th Street, New York, NY 10032, USA; jrs88@cumc.columbia.edu.

Submitted: February 28, 2018

Accepted: April 8, 2018

Citation: Paavo M, Zhao J, Kim HJ, et al. Mutations in *GPR143/OA1* and *ABCA4* inform interpretations of short-wavelength and near-infrared fundus autofluorescence. *Invest Ophthalmol Vis Sci.* 2018;59:2459–2469. <https://doi.org/10.1167/iovs.18-24213>

PURPOSE. We sought to advance interpretations and quantification of short-wavelength fundus autofluorescence (SW-AF) emitted from bisretinoid lipofuscin and near-infrared autofluorescence (NIR-AF) originating from melanin.

METHODS. Carriers of mutations in X-linked *GPR143/OA1*, a common form of ocular albinism; patients with confirmed mutations in *ABCA4* conferring increased SW-AF; and subjects with healthy eyes were studied. SW-AF (488 nm excitation, 500–680 nm emission) and NIR-AF (excitation 787 nm, emission >830 nm) images were acquired with a confocal scanning laser ophthalmoscope. SW-AF images were analyzed for quantitative autofluorescence (qAF). Analogous methods of image acquisition and analysis were performed in albino and pigmented *Abca4*^{-/-} mice and wild-type mice.

RESULTS. Quantitation of SW-AF (qAF), construction of qAF color-coded maps, and examination of NIR-AF images from *GPR143/OA1* carriers revealed mosaics in which patches of fundus exhibiting NIR-AF signal had qAF levels within normal limits whereas the hypopigmented areas in the NIR-AF image corresponded to foci of elevated qAF. qAF also was increased in albino versus pigmented mice. Although melanin contributes to fundus infrared reflectance, the latter appeared to be uniform in en face reflectance images of *GPR143/OA1*-carriers. In patients diagnosed with *ABCA4*-associated disease, NIR-AF increased in tandem with increased qAF originating in bisretinoid lipofuscin. Similarly in *Abca4*^{-/-} mice having increased SW-AF, NIR-AF was more pronounced than in wild-type mice.

CONCLUSIONS. These studies corroborate RPE melanin as the major source of NIR-AF but also indicate that bisretinoid lipofuscin, when present at sufficient concentrations, contributes to the NIR-AF signal. Ocular melanin attenuates the SW-AF signal.

Keywords: fundus autofluorescence, near-infrared autofluorescence, short-wavelength autofluorescence, *GPR143/OA1*, X-linked albinism, recessive Stargardt disease, *ABCA4*

The clinical diagnosis and monitoring of retinal disease often relies on changes in the patterns and intensities of retinal autofluorescence (AF). This autofluorescence is commonly imaged at the fundus by confocal scanning laser ophthalmoscopy (cSLO) with excitation by short-wavelength (SW-AF; 488 nm) light. The cellular source, spectral features, and age relationship of SW-AF are indicative of an origin from visual cycle products that accumulate in RPE as lipofuscin.^{1,2} These bisretinoid fluorophores are a family of retinaldehyde-adducts that form nonenzymatically in photoreceptor cells and are transferred within phagocytosed outer segment membrane to RPE cells. Bisretinoids form in all healthy eyes, but are particularly abundant in recessive Stargardt disease (STGD1) due to mutations in the *ABCA4* (ATP-binding cassette transporter 4) gene.³ A second AF originating in large part from RPE melanin is emitted with near-infrared (787 nm) excitation (NIR-AF).^{4,5}

In the macula of a healthy subject, the distributions of the NIR-AF and SW-AF signals exhibit different patterns. In particular, the NIR-AF emission is high centrally due to

increased optical density of melanin in an area approximately 8° in diameter.^{4,6,7} On the other hand, the SW-AF signal in central macula and especially the fovea is reduced due to absorption of the excitation light by macular pigment.⁸ Peripheral to the macula, the NIR-AF and SW-AF signals are relatively uniform.

In addition to the high foveal NIR-AF signal that corresponds to elevated melanin optical density in RPE,^{4,6,9,10} the assertion that NIR-AF originates primarily from RPE melanin is based on research showing that the NIR-AF signal is bright within the window-defect created by a full-thickness macular hole.⁴ In addition, melanocytic choroidal nevi fluoresce under NIR-AF excitation,^{4,10} as do melanosomes isolated from RPE,⁵ cutaneous melanin,¹¹ and the pigmented epithelium of the iris.⁴ Conversely, in the presence of RPE atrophy such as occurs in STGD1 due to mutations in the *ABCA4* gene, central lesions present as areas of reduced SW- and NIR-AF due to a loss of RPE.¹²

Nevertheless, the origin of NIR-AF is not fully understood. Bone spicule-like pigmentation in the peripheral fundus of

retinitis pigmentosa (RP) patients can be readily apparent in color fundus photographs while being hypoautofluorescent in NIR-AF images and nonreflective in infrared reflectance (IR-R) images.¹³ Moreover, the prevailing assumption that NIR-AF originates only from melanin is a barrier to an explanation for why bright AF rings in SW-AF images of RP patients are also visible in NIR-AF images (787 nm).^{7,13,14} Other observations also have been puzzling. For instance, although both modalities are thought to originate from RPE, discrepancies can occur as to the boundaries of atrophy in recessive STGD1, with zones of RPE atrophy being larger in NIR-AF images than in SW-AF images.^{9,15} Also unexplained is why on the temporal side of a demarcation line attributable to the optic fissure, SW-AF and NIR-AF signals are increased in STGD1 patients while this difference was not detectable in healthy control eyes.¹⁶

As a component of our efforts to advance clinical interpretations of SW-AF and NIR-AF images, we studied NIR-AF and SW-AF images in patients carrying mutations in *ABCA4* that confer increased SW-AF intensity. We also examined fundus images acquired from female carriers of *GPR143/OA1* mutations that are the most common cause of ocular albinism. Random X-inactivation of the *OA1/GPR143* gene in RPE cells of carriers of *OA1/GPR143* mutations causes melanin pigmentation in retina to acquire a mosaic pattern. Several mouse lines differing in their content of RPE melanin and lipofuscin also were studied.^{7,12,16-19} While confirming that melanin is the major source of NIR-AF, we demonstrated that retinal lipofuscin imaged as SW-AF can contribute to NIR-AF intensities. Conversely, ocular pigmentation modulates SW-AF intensities. To the best of our knowledge, this study is the first to present NIR-AF images and quantitative AF (qAF) of *GPR143/OA1* mutation carriers.

METHODS

Patients, Clinical Evaluation, and Genetic Testing

A retrospective analysis was performed of fundus AF images from five carriers of mutations in the X-linked ocular albinism gene *GPR143/OA1* (Table 1). Three of the carriers (patient [P]1, 2, 3) were the daughters of a *GPR143/OA1* male proband (P6) who presented to the clinic. The fourth and the fifth carriers (P4, P5) were not related to the aforementioned family. All subjects had a comprehensive ophthalmological examination by a retina specialist and assessment of best-corrected visual acuity. For genetic testing, blood was collected from all patients and genomic DNA was extracted from blood lymphocytes using a standard protocol.

Direct Sanger sequencing revealed that the three sisters from the same family (P1, P2, P3) were all heterozygous carriers of a novel mutation c.461del_T (p.Ile154fs) in *GPR143/OA1*. All nine exons were amplified and directly sequenced, and no other variants were found. Sequence analysis of *GPR143/OA1* in P4 disclosed heterozygosity for the c.455+3A>G mutation. Results of genetic testing were not available for P5; the clinical diagnosis was based on iris transillumination and typical RPE mosaicism in the fundus.

P6 (father of P1, P2, P3) was hemizygous for the mutation c.461del_T (p.Ile154fs) in *GPR143/OA1* and is described in the Supplement.

A prospective analysis of fundus AF images acquired from 25 patients (age range 8.3–51.5 years) with clinically and genetically confirmed diagnosis of STGD1 was carried out. Images of patients with advanced disease (appreciable loss of the NIR-AF signal throughout the 30° field) were not included. Clinical, demographic, and genetic data are presented in Table 1. At least one known mutation in the *ABCA4* gene was

detected in all patients by direct sequencing. Two (expected) *ABCA4* mutations were detected in 22 (88%) of 25 patients. The control group consisted of 15 individuals without a history of eye disease. The mean age was 34.9 years (range 12.7–52.7 years) and 10 subjects identified themselves as Caucasian, 3 as Hispanic, 1 Asian, and 1 African American. Both groups underwent a comprehensive eye examination.

All procedures adhered to the tenets of the Declaration of Helsinki and written informed consent was obtained from all patients after full explanation of the procedures. The study was carried out with the approval of the Institutional Review Board of Columbia University, and all patients were enrolled in accordance with the tenets set out in the Declaration of Helsinki. Informed consent was obtained before enrollment.

Image Acquisition and Analysis in Patients and Subjects

SW-AF (blue AF; 488 nm excitation, 500–680 nm emission) images (55° × 55° and 30° × 30° fields) were acquired with cSLO (Spectralis HRA+OCT; Heidelberg Engineering, Heidelberg, Germany) and saved in normalized mode. SW-AF images for qAF analysis were obtained with a Spectralis modified by the insertion of an internal fluorescent reference.²⁰ Videos of either 9 or 12 frames were captured in the high-speed mode (8.9 frames/s) and saved in non-normalized mode (i.e., without histogram stretching). Protocols used for qAF have been published.³

To calculate qAF and generate qAF maps, gray levels (GLs) in predetermined segments centered on the fovea (7°–9° eccentricity) were normalized to GLs in the internal fluorescent reference while standardizing for the zero GL, the magnification (refraction), and ocular media absorption.²¹ Values in the eight segments were averaged to obtain qAF₈. The normative database of healthy eyes (374 eyes; age range, 5–60 years) has been described.²²

NIR-AF images (55° × 55° and 30° × 30° field) were obtained with an HRA2-SLO (Heidelberg Engineering; excitation 787 nm, emission >830 nm; without injection of dye) and a sensitivity of 96. The NIR-AF signal acquired with the HRA2-SLO is more robust than with the Spectralis because in the latter the detection channel is divided between the SD-OCT and NIR-AF modalities. The eye-tracking function was used and 100 single frames were averaged. Images were saved in both normalized and non-normalized mode. The image of the right eye was chosen for analysis, but if that image was not usable, the left eye was analyzed. Images were selected based on sufficient image quality and STGD1 images with extensive flecks or atrophy were not included.

To quantify NIR-AF in 30° × 30° fields, non-normalized images of STGD1 patients (25) and healthy control eyes (15) were imported into an open source image analysis software (Fiji; National Institutes of Health, Bethesda, MD, USA). The straight-line analysis tool was used to draw a horizontal line through the fovea for the full width of the image and GL values were acquired along this horizontal axis. The points on the horizontal axis first presented distance from fovea in pixels and were later converted into micrometers from fovea using the scaling factor (μm/pixel) provided by Heidelberg software. The GL values were then adjusted by subtracting the NIR-AF image GL offset-value generated by the Heidelberg software. GL profiles of STGD1 patients and age-matched healthy eyes were then plotted as a function of distance along the x-axis in the temporal (0 to −4 mm) and nasal (0 to +4 mm) direction relative to the fovea. The profiles were aligned so that the fovea was always at position zero (0).

SD-OCT images were acquired in high-resolution mode (9 mm foveal and volume scans) and registered to a simulta-

TABLE 1. Clinical, Demographic, and Genetic Data

Patient	Age at Visit	Eye Analyzed	Ethnicity	BCVA*		Genetic Variants
				OD	OS	
OA1/GPR143						
1	13.5	OA	Hispanic	0	0	Heterozygous mutation GPR143/OA1 gene, c.461del_T (p.Ile154fs)
2	17.3	OA	Hispanic	0	0	Heterozygous mutation GPR143/OA1 gene, c.461del_T (p.Ile154fs)
3	21.7	OA	Hispanic	0	0	Heterozygous mutation GPR143/OA1 gene, c.461del_T (p.Ile154fs)
4	34.6	OA	Asian	0	0	Heterozygous mutation GPR143/OA1 gene, c.455+3A>G
5	20.1	OA	Caucasian	0	0	Not available
6	43.1	OA	Hispanic	1	1	Hemizygous mutation GPR143/OA1 gene, c.461del_T (p.Ile154fs)
STGD1						
1	14.3	OD	Caucasian	0.7	1	p.G1961E p.P1380L
2	8.3	OD	Indian	0.5	0.6	p.R653C p.G1961E
3	12.9	OD	Caucasian	0.9	0.9	p.[L541P;A1038V] p.L2027F
4	17.2	OD	Caucasian	0.1	0.1	p.R1108C p.Q1412
5	17.7	OD	Caucasian	0.7	0.7	p.G1961E
6	18.5	OD	Caucasian	0.8	0.9	p.A1773V p.G1961E
7	21.6	OD	Caucasian	0.7	0.7	p.G1961E
8	22.6	OD	Caucasian	0.3	0.2	p.R602W p.N1868I
9	24.5	OD	Caucasian	0.9	0.4	p.G1961E p.N96D
10	25.9	OS	Caucasian	0.7	0.7	p.G1961E
11	26.8	OS	Caucasian	1.17	1.17	p.G1961E p.L541P
12	27.8	OD	Caucasian	0.7	0.6	p.G1961E p.C2150R
13	29.9	OD	Caucasian	0.9	0.9	c.3050+5G>A p.G1961E
14	31.6	OS	Afro Arab	0.1	0.1	p.R1300 p.R2106C
15	36.3	OD	Caucasian	0.7	0.1	p.N1799D p.N1868I
16	45	OD	Caucasian	0.4	0.4	p.R2106C p.[L541P;A1038V]
17	46.6	OD	Indian	0.3	0.6	p.T1526M c.1938-822_1938-808del15
18	50.7	OD	Caucasian	0.4	0.4	p.R2077G p.R2107H
19	51.5	OS	Caucasian	0.1	0.1	p.N1868I p.P1380L
20	45.8	OS	Caucasian	0.17	0.17	p.G1961E p.G1961E
21	21.9	OD	Caucasian	0.1	0.1	p.G1961E p.N96D
22	25.4	OS	Caucasian	0.7	0.7	p.G1748E p.R2106H
23	15.2	OS	Caucasian	0	0.1	p.G1961E p.V615A
24	11.4	OD	Caucasian	1	1.3	p.[L541P;A1038V] c.768+358C>T
25	13.5	OD	Caucasian	1	0.3	p.V989A c. 2918+5G>A

* Best-corrected visual acuity logMAR equivalent.

neously acquired near-infrared reflectance (IR-R; 820 nm) image using the Spectralis HRA+OCT. The Heidelberg Eye Explorer software was used to determine mean foveal thickness using the central subfield (diameter 1 mm) of the Early Treatment Diabetic Retinopathy Study grid.²³ The control group consisted of 51 females without evidence of eye disease (aged 7–55, mean age 29) of whom 10 identified as Asian, 7 African American, 7 Hispanic, 4 Indian, and 23 white.

Swept-source widefield OCT (12 mm, 9 mm, and 6 mm cube and angiography scans) images were obtained with the Cirrus PLEX Elite 9000 (Carl Zeiss Meditec, Jena, Germany) and en face images adjusted to the level of RPE were created with Cirrus PLEX Elite 9000 software. Color fundus photographs were obtained with a FF 450plus Fundus Camera (Carl Zeiss Meditec). Ultra-widefield high-resolution optomap images were also captured (Optos Daytona; Optos, Inc., Marlborough, MA, USA) in the composite color and AF (excitation 532 nm) mode.

Mice

Albino *Abca4/Abcr* null mutant mice (*Abca4*^{-/-}), homozygous for Rpe65-Leu450, were reared and genotyped²⁴ (Table 2). Agouti *Abca4*^{+/-} (129S-*Abca4*tm1Ght/J; Rpe65-Leu450) and agouti *Abca4*^{+/+} (129S1/SvImJ; Rpe65-Leu450) were purchased from The Jackson Laboratory (Bar Harbor, ME, USA) and bred in-house. Agouti *Rdb8*^{-/-}*Abca4*^{-/-} mice (Rpe65-Leu450) were acquired as a gift from Krzysztof

Palczewski, Case Western Reserve University (Cleveland, OH, USA). Black C57BL/6J, and albino C57BL/6J^{c2j} wild-type mice (Rpe65-Met450) were purchased from The Jackson Laboratory. The research was approved by the Institutional Animal Care and Use Committee and adhered to the ARVO Statement for the Use of Animals in Ophthalmic and Vision Research.

TABLE 2. Mouse Strains Used in These Studies

Mouse Line	Melanin Status	Bisretinoid Status	Rpe65-450 Variant
<i>Abca4</i> ^{-/-}	Albino	Elevated relative to albino <i>Abca4</i> ^{+/+}	Leu-450*
<i>Abca4</i> ^{+/+}	Albino		Leu-450
<i>Abca4</i> ^{-/-}	Agouti	Elevated relative to agouti <i>Abca4</i> ^{+/+}	Leu-450
<i>Abca4</i> ^{+/+}	Agouti		
<i>Rdb8</i> ^{-/-} <i>Abca4</i> ^{-/-}	Agouti	Elevated relative to agouti <i>Abca4</i> ^{-/-}	Leu-450
<i>C57BL/6J</i> ^{c2j}	Albino	Reduced relative to black C57BL/6J	Met-450†
<i>C57BL/6J</i>	Black		<i>Met-450</i>

* Leucine at position 450.

† Methionine at position 450.

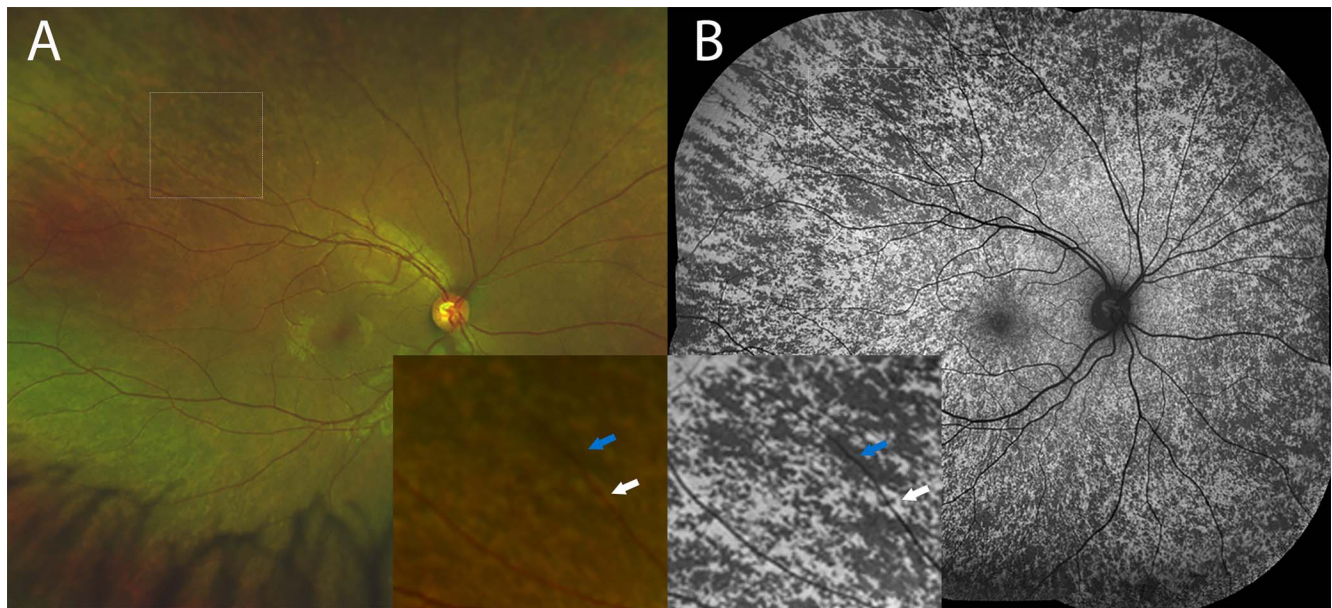


FIGURE 1. *GPR143/OA1* carrier (Patient 3). (A) Pseudocolor (Optos System). (B) SW-AF (488 nm) (Heidelberg Spectralis), composite image. Pigmented (*blue arrow*) and hypopigmented (*white arrow*) areas are indicated in pseudocolor and SW-AF images.

Image Acquisition and Analysis in Mice

Mice were anesthetized with an intraperitoneal injection of ketamine (100 mg/kg) and xylazine (10 mg/kg). Protocols for positioning, pupillary dilation, temperature monitoring, and placement of contact lens have been described.²⁵ After visual pigment bleaching, fundus images (55° lens) were acquired with a cSLO (Spectralis HRA+OCT) equipped with an incident laser beam of 0.98 mm and an internal fluorescence reference.²⁵

Nine successive frames were acquired in high-speed mode (8.9 images/s), using a sensitivity of 95 to 100; the frames were averaged and saved in the non-normalized mode. Fundus SW-

AF images were analyzed as described²⁵ and qAF was calculated by calibrating GLs, in predetermined fundus segments, to the GL of the fluorescent reference (GL_R).⁸ All mice were exposed to only a single occasion of imaging.

High-resolution NIR-AF (787 nm excitation, >830 nm emission) images were acquired at a sensitivity of 105 and after averaging 100 frames with background subtraction, the images were saved in non-normalized mode. GLs were measured using ImageJ (<http://imagej.nih.gov/ij/>; provided in the public domain by the National Institutes of Health, Bethesda, MA, USA). Between-session coefficient of repeatability (Bland-Altman) of NIR-AF GL values was 3.5%.

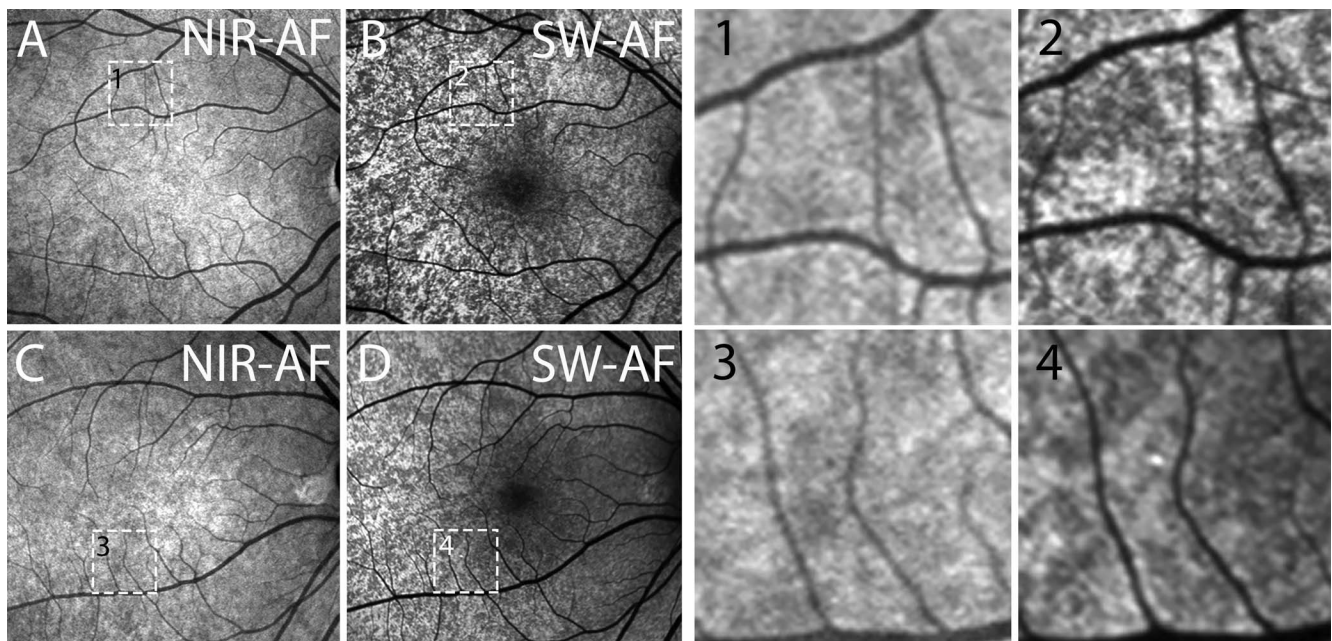


FIGURE 2. NIR-AF (787 nm) and SW-AF (488 nm) images of *GPR143/OA1* carriers. P3 (A, B) and P4 (C, D). (Spectralis, Heidelberg Engineering). Areas in the rectangles in (A–D) are magnified in images in 1–4.

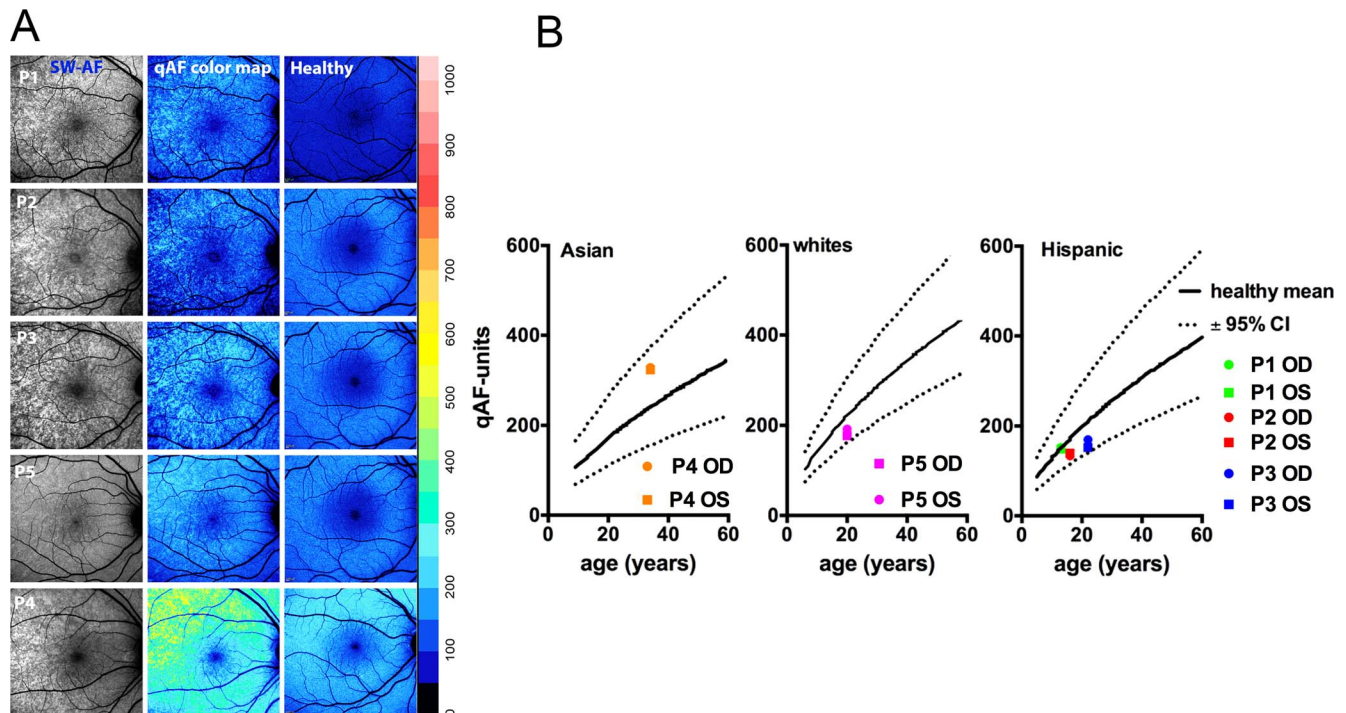


FIGURE 3. (A) SW-AF (488 nm) images and color-coded qAF images of *GPR143/OA1* carriers (P1–P5) and age-matched healthy eyes. The age-matched healthy subjects are aged 11.3 (P1), 20.1 (P2, P3, P5), and 32.6 (P4). Color codes are scaled from 0 to 1200 as indicated. (B) qAF in Asian, white, and Hispanic *GPR143/OA1* carriers (colored symbols) (P1–P5) and age-matched healthy subjects (mean, *solid black line*; and 95% confidence intervals, *dashed lines*). qAF was measured in eight circularly arranged segments, 7° – 9° from the fovea (qAF₈).

Quantitative HPLC

Mouse eyecups (4–6 per sample) were homogenized and extracted for quantitation by HPLC (Alliance system; Waters, Corp, Milford, MA, USA) as previously described.²⁶

Statistics

Analyses were performed using Prism 5 (GraphPad Software, La Jolla, CA, USA) and the statistical tests as indicated.

RESULTS

Carriers of *GPR143/OA1* Mutations

The five female carriers of *GPR143/OA1* mutations (P1–P5; mean age 21.7, age range 13.5–34.6) were asymptomatic, with the exception of P3 who complained of difficulty seeing in the dark. All carriers had best-corrected visual acuity of 20/20. The three sisters (P1, P2, P3) showed no iris transillumination defects on anterior segment examination; for P4 those data were not available. Patient 5 exhibited iris transillumination on slit-lamp examination.

The five *GPR143/OA1* carriers also exhibited nonuniform fundus pigmentation with radially directed hypopigmented streaks stretching from the macular area to the peripheral fundus in SW-AF images (Figs. 1A, 1B) as previously observed.²⁷ The elevated NIR-AF emission typically observed in central fundus of healthy eyes, was less obvious in these individuals (Figs. 2A, 2C). Additionally, in *OA1* carriers, subtle patterns in fundus NIR-AF and SW-AF images were visible (Fig. 2). Specifically, the units of the mosaic exhibiting NIR-AF signal (Figs. 2A, 2C) were associated with lower SW-AF (Figs. 2B, 2D), whereas the hypopigmented areas in the NIR-AF image (Figs. 2A, 2C) corresponded to foci of readily detectable SW-AF (Figs. 2B, 2D).

GPR143/OA1 Carriers: Quantitative Fundus AF

To further understand patterns of AF, we quantified SW-AF intensities using qAF^{20,21,28} protocols. Levels of qAF₈ (7° – 9° eccentricity) in *GPR143/OA1* carriers fell within the 95% confidence intervals for age-matched healthy eyes (Fig. 3B). Comparison of *GPR143/OA1* carriers and age-matched healthy subjects using color-coded qAF maps scaled to a qAF range of 0 to 1200, revealed that in carriers, the pigmented units of the mosaic corresponded to the level of normal AF, whereas the hypopigmented areas exhibited significantly higher focal areas of SW-AF (Fig. 3A).

Carriers of *GPR143/OA1* Mutations: SD-OCT and En Face OCT Images

All of the carriers exhibited normal foveal depression with no signs of foveal hypoplasia (Fig. 4). The carriers had a moderately reduced central subfield foveal thickness (mean $253.0 \mu\text{m} \pm 18.42 \text{ SD}$, 7.519 SEM) as compared with the control group (mean $265.9 \pm 18.57 \text{ SD}$, 2.600 SEM), but the difference was not statistically significant ($P > 0.05$, unpaired two-tailed *t*-test).

En face fundus images extracted at the level of RPE for the four carriers (P1, P2, P3, P5) revealed reflectivity that was homogeneous (Fig. 4). Melanin is a major reflective element in the RPE^{29–31}; nevertheless, we did not observe transmission into the choroid in association with melanin-deficient patches in the eyes of *GPR143/OA1* carriers (Fig. 4). En face images for P4 were not available.

STGD1/*ABCA4* Disease: NIR-AF Signal

We have previously reported that SW-AF intensities measured as qAF are considerably elevated in retinal disease caused by



FIGURE 4. Images obtained from *GPR143/OA1* carriers (P1, 2, 3, 4, 5) and a healthy eye (age 29.6 years) by IR-R and horizontal SD-OCT (Spectralis). En face OCT images at levels of RPE are shown (swept-source widefield OCT), and at the bottom an SS-OCT scan showing the segmentation for RPE en face slab.

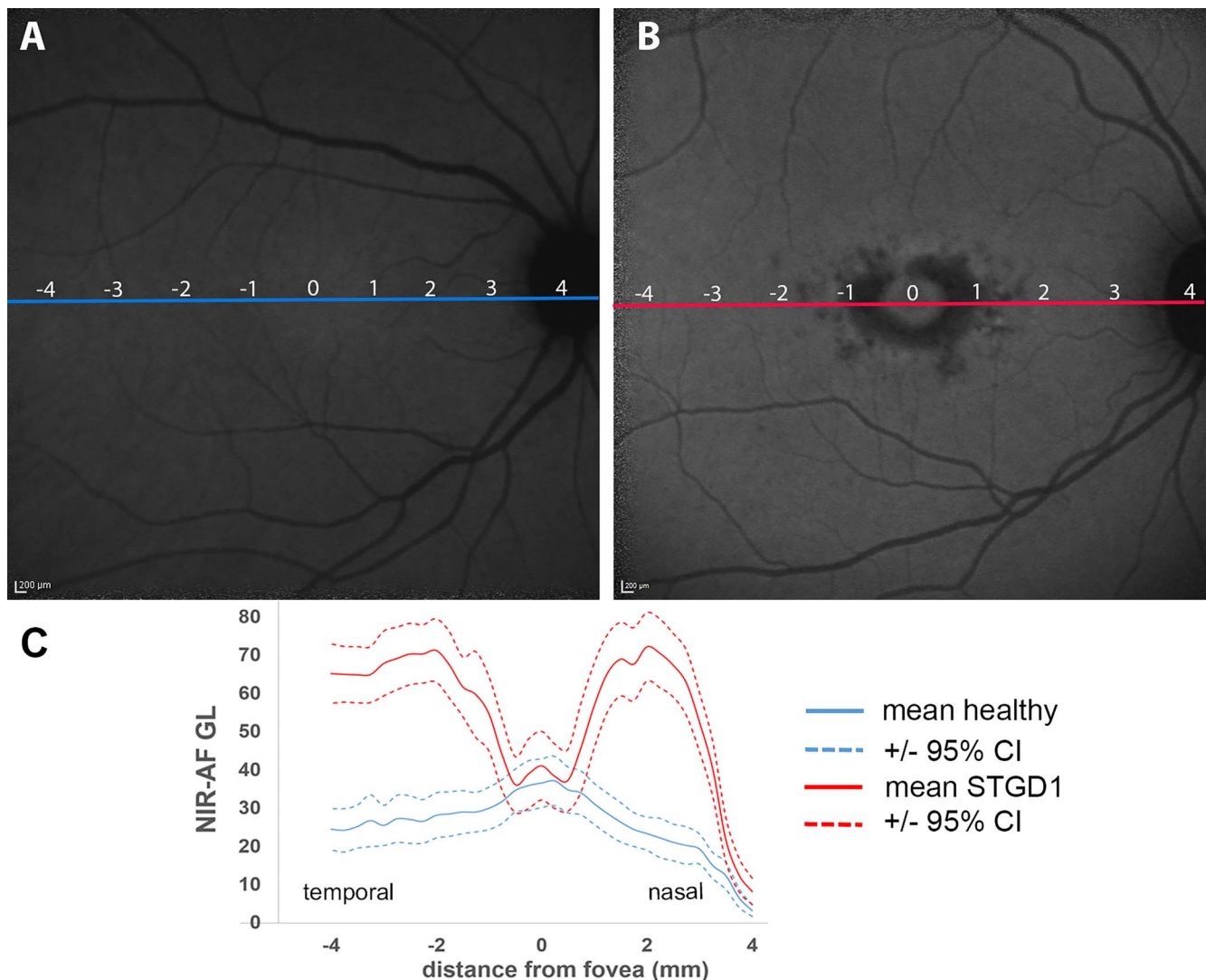


FIGURE 5. NIR-AF in STGD1. (A, B) NIR-AF images acquired from a healthy subject (age 48.3 years) (A) and STGD1 patient (31.6 years) (B). (C) NIR-AF intensity profiles presented as mean normalized GLs (solid lines) together with 95% confidence intervals (CIs) and plotted as a function of temporal-to-nasal distance along a horizontal line through the fovea in healthy subjects ($n = 15$) and STGD1 patients ($n = 25$).

ABCA4 mutations,³ and we have speculated as to an accompanying upturn in NIR-AF in these patients.¹⁶ To more fully examine this issue, GL NIR-AF intensities were measured in STGD1 and healthy retina at 1-mm intervals (nine positions) along a horizontal axis beginning at the fovea and proceeding temporally (0 to -4) and nasally (0 to $+4$) (Fig. 5). As expected, healthy eyes exhibited an increase in NIR-AF signal in a zone approximately 8° (2.3 mm from fovea) in diameter centered on the fovea. Within the same area, NIR-AF signal was reduced in the STGD1 patients because of central atrophy. Outside the fovea, GL values were consistently elevated in the STGD1 cohort, with the differences in GL values between the STGD1 and healthy eyes being statistically significant at all positions ($P < 0.05$, ANOVA and Sidak's multiple comparison test) (except at the 4-mm nasal position due to absent NIR-AF signal at the optic disc). The difference was as much as 3-fold (2 mm nasal to fovea).

Fundus AF in Mice

Using mice varying in melanin and RPE lipofuscin levels, together with instrumentation (Spectralis HRA+OCT) used in

humans,²⁵ we sought information supporting our observations in the human patients (Fig. 6). We first assessed for relationships among age (2–9 months) and genotype-related increases in RPE lipofuscin (measured as qAF) and increases in NIR-AF. Agouti *Abca4*^{-/-} mice serve as a model of accelerated formation of bisretinoid lipofuscin; the inadequate clearance of retinaldehyde in these mice results in bisretinoid accumulation that is approximately 3-fold higher in *Abca4*^{-/-} mice than wild-type^{26,32,33} (Fig. 6A). As shown in Figure 6, the NIR-AF signal in the agouti *Abca4*^{-/-} mice having elevated RPE lipofuscin (increased SW-AF) was greater than in agouti *Abca4*^{+/+} mice on the same genetic background (Fig. 6A). In those fundus images in which the SW-AF signal in *Abca4*^{+/+} mice appeared just as bright or brighter than in the *Abca4*^{-/-} mouse (Fig. 6A), it is noted that the internal fluorescent reference, visible in the image, was also brighter, indicating that the image was acquired using a greater sensitivity setting. Plots of NIR-AF versus SW-AF (age 2–9 months) in agouti *Abca4*^{-/-} (72.4 ± 8 , SE) versus *Abca4*^{+/+} (156 ± 63 , SE) mice revealed different slopes (*t*-test, $P < 0.05$). Moreover, for the same age interval, the greater change in SW-AF (x-axis) in the agouti *Abca4*^{-/-}

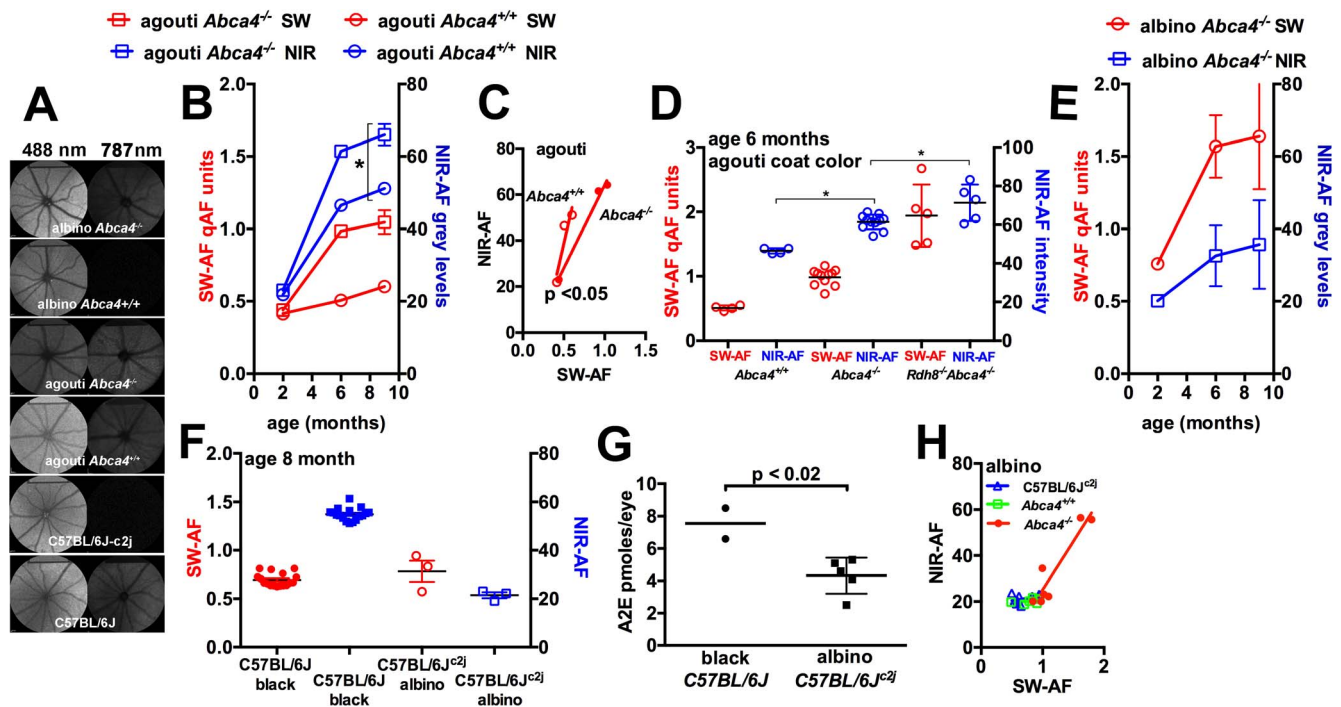


FIGURE 6. Fundus AF and HPLC analysis of mouse eyes. (A) SW-AF (488 nm) and NIR-AF (787 nm) images of mouse fundus. *Abca4*^{-/-} and wild-type (*Abca4*^{+/+}) albino mice and mice with an agouti coat color were imaged as indicated. The internal AF reference is visible in the top of the image. Note that in the case of the *Abca4*^{+/+} mouse, the fundus has relatively high GLs, but the internal fundus AF reference is also brighter, reflecting lower qAF levels. (B–G) Analysis of SW-AF and NIR-AF images acquired in mice at indicated ages. SW-AF is quantified as qAF units and NIR-AF as GLs. (B) SW-AF and NIR-AF plotted as a function of age in agouti *Abca4*^{-/-} and *Abca4*^{+/+} mice. (C) Plots of NIR-AF and SW-AF (age 2–9 months) in agouti *Abca4*^{-/-} and *Abca4*^{+/+} mice reveal different slopes (*t*-test, $P < 0.05$), indicating a greater increase in NIR-AF in mice exhibiting increased SW-AF (*Abca4*^{-/-}). (D) SW-AF and NIR-AF in agouti *Abca4*^{+/+}, *Abca4*^{-/-}, and *Rdh8*^{-/-}/*Abca4*^{-/-} mice, indicating increases in NIR-AF intensity as SW-AF is elevated. (E) SW-AF and NIR-AF plotted as a function of age in albino *Abca4*^{-/-} mice. (F) NIR-AF plotted versus SW-AF for black C57BL/6J and albino C57BL/6J^{c2j} mice (age 8 months). (G) HPLC quantitation of the bisretinoid A2E in black C57BL/6J and C57BL/6J^{c2j} mice. (H) Plotting of NIR-AF versus SW-AF for albino wild-type mice (C57BL/6J^{c2j}, *Abca4*^{+/+}) and *Abca4*^{-/-} mice (age 4 and 6 months). Means \pm SEM are based on 2 to 11 mice.

mice resulted in a greater change in NIR-AF (y-axis) than in the agouti *Abca4*^{+/+} mice (Fig. 6B).

We also recorded AF levels in agouti *Rdh8*^{-/-}/*Abca4*^{-/-} double knockout mice. Absence of *Rdh8* (retinol dehydrogenase 8) causes bisretinoid levels to undergo additional escalation as compared with the single knockout *Abca4*^{-/-} mice.^{34,35} The stepwise increase in SW-AF (qAF) in the agouti *Abca4*^{+/+}, *Abca4*^{-/-}, and *Rdh8*^{-/-}/*Abca4*^{-/-} mice was paralleled by increases in NIR-AF intensity (Fig. 6E).

To test for an NIR-AF signal in the absence of melanin, we also studied albino *Abca4*^{-/-} mice.

As can be expected of an imaging modality that is considered to originate in melanin, NIR-AF was more robust in agouti *Abca4*^{-/-} mice than in albino *Abca4*^{-/-} mice (Figs. 6B versus 6E). Nevertheless, despite the absence of melanin, the NIR-AF signal in the albino *Abca4*^{-/-} mice increased in tandem with the age-associated increase in the SW-AF signal (Fig. 6E).

Because in the hypopigmented areas of the fundus of *GPR143/OA1* carriers, SW-AF intensities were increased, we also compared qAF in albino mice. Consistent with observations in the *GPR143/OA1* carriers, SW-AF intensity (qAF) in the albino *Abca4*^{-/-} mice was elevated relative to the age-matched agouti *Abca4*^{-/-}. This difference at first glance was incongruous given our previously reported evidence that bisretinoid measured as A2E, is higher in the agouti.²⁶ Thus, we also compared black C57BL/6J with albino C57BL/6J^{c2j} mice; black C57BL/6J and albino C57BL/6J^{c2j} mice are genetically identical except that the albino C57BL/6J^{c2j} are homozygous for the mutation in the tyrosinase gene (*c/c*). The levels of qAF in SW-AF images were similar in black C57BL/6J and albino C57BL/

6J^{c2j} mice (Fig. 6E), even though we also showed by chromatographic quantitation of the bisretinoid A2E, that the latter are present in lesser amounts in the albino eye (Fig. 6G). Reduced HPLC quantified bisretinoid in the albino mice is due to loss associated with photooxidation and photodegradation.²⁵ Thus, the more intense SW-AF in the albino would undoubtedly be due to the greater irradiance received by the RPE cell fluorophores in the eyes lacking melanin and due to light reflected by the sclera.²⁶ By plotting NIR-AF values as a function of SW-AF (age 4 and 6 months) for albino wild-type (*Abca4*^{+/+}, C57BL/6J^{c2j}) and *Abca4*^{-/-} mice, it was apparent that NIR-AF levels did not change when SW-AF intensity was limited to levels less than 1 qAF-unit. It is also notable that NIR-AF was more intense in mice having a black (i.e., C57BL/6J) versus agouti (*Abca4*^{-/-}) coat color (Fig. 6A versus 6F).

DISCUSSION

The most common form of ocular albinism is caused by mutations in the heterotrimeric G protein-coupled receptor, *GPR143/OA1*. *OA1* loss of function does not impair the activity of tyrosinase, the enzyme controlling the production of melanin, but reduces the expression of premelanosome protein (PMEL), a major melanosomal structural protein that provides the melanosome fibrillar matrix for melanin polymerization as it is synthesized.^{36–38} Consequently, melanin is synthesized but melanosomes are grossly enlarged and reduced in number in the presence of *GPR143/OA1* mutations³⁹ and the organization of melanin in the melanosomes is altered.^{37,38}

This condition contrasts with that in the albino mice that lack melanin synthesis.

Melanin Is the Major Contributor to the NIR-AF of the Fundus

In this study, we have added NIR-AF imaging to the examination of the fundus in *GPR143/OA1* carriers. In these individuals, small-scale patches of NIR-AF darkness alternated with similar-sized foci of brightness in the NIR-AF images. The signal for NIR-AF originates from melanin, at least in part,⁴ and thus the darkness in the NIR-AF images of *GPR143/OA1* carriers corresponded to nonpigmented areas of the fundus, while brightness corresponded to the presence of melanin pigment, with the signal primarily originating in the RPE melanin (as opposed to choroidal melanin). This pattern of AF in the NIR-AF images of *GPR143/OA1* carriers together with the NIR-AF signal observed in mice, supports previous reports indicating that NIR-AF originates from melanin.⁴

NIR-AF Signal Can Undergo Increases in Tandem With SW-AF

In STGD1/*ABCA4* patients, we confirmed that the increase in SW-AF intensity was paralleled by a generalized increase in NIR-AF signal.^{9,16} Similarly, the NIR-AF signal in agouti *Abca4*^{-/-} mice was elevated relative to the NIR-AF signal in agouti *Abca4*^{+/+} mice. By way of explaining the enhanced NIR-AF, it is conceivable that NIR-AF may be increased if lipofuscin-containing organelles in the RPE modulate the NIR-AF signal originating from melanin. For instance, the broadband absorbance spectrum of melanin leads to density-dependent self-absorbance of the fluorescence emitted by neighboring melanin molecules.⁴⁰ Accordingly, quenching of the NIR fluorescence emission by secondary absorbance could be reduced if the packing density of melanosomes was altered by the interspersions of melanosomes with lipofuscin storage bodies. Under these circumstances, more pronounced release of the fluorescence emission of melanin could occur. Nevertheless, this mechanism does not account for the observation that in albino *Abca4*^{-/-} mice, fundus NIR-AF intensities were elevated in tandem with increases in SW-AF even in the absence of melanin. The NIR-AF difference in albino *Abca4*^{-/-} versus albino wild-type mice, both of which are deficient in the tyrosinase gene required for melanin synthesis, indicates that bisretinoid is not stimulating increased melanin synthesis, as has been postulated previously.⁴¹ Similarly, an increase in numbers of melanosomes paralleling a rise in NIR-AF intensity was not observed in pigmented *Abca4*^{-/-} mice.⁴² An alternative explanation is that bisretinoid can contribute to the NIR-AF signal.

An age-related increase in the perifoveal NIR-AF due to a contribution from increasing levels of lipofuscin could explain the age-related decline in the foveal-to-perifoveal NIR-AF ratio.⁴ An increase in NIR-AF intensity also occurs in conjunction with the SW-AF rings that are often observed in the fundus of retinitis pigmentosa patients.⁷ The hyperautofluorescent rings in NIR-AF images are unlikely to be due to a change in transmission in the retinal layers that are anterior to the RPE (unmasking), because tissue absorption at wavelengths between 600 and 1300 nm is relatively low.⁴³ Pigmentary changes corresponding to the distribution of the hyperautofluorescent NIR-AF ring are not observed in color fundus photographs and changes in the thickness of RPE/Bruch's membrane-attributable hyperreflective band is not visible by SD-OCT as has been reported at the borders of geographic atrophy in AMD.^{44,45}

We note, however, that melanin is the major source of NIR-AF. Indeed, lower levels of RPE lipofuscin, such as those responsible for SW-AF in albino wild-type mice, do not make a detectable difference to NIR-AF intensities probably because the contribution to the NIR-AF signal in the wild-type is minor in comparison with melanin (Fig. 6).⁵ This observation is likely applicable to the healthy human eye.

IR-R and Melanin

Melanin is also responsible for IR-R by the RPE monolayer²⁹⁻³¹ in fundus images. Although in NIR-AF images of *GPR143/OA1* carriers the fundus presented as a mosaic of variable AF, a mosaic of differing reflectivity was not observed in en face OCT images at the level of RPE. Also, in horizontal SD-OCT scans, zones of increased transmission into the choroid were not observed. Thus, the impact of *GPR143/OA1* deficiency on the NIR-AF and reflectivity properties of the melanosome are not the same.⁴⁶

SW-AF Signal Is Attenuated by the Presence of RPE Melanin

With examination of the SW-AF images acquired from *GPR143/OA1* carriers, we found that the foci that were less intense in SW-AF images (dark) were associated with bright focal areas in NIR-AF images, indicating that the SW-AF signal is attenuated by the presence of RPE melanin. Conversely, SW-AF appeared brighter in areas characterized by an absence of melanin. This is consistent with the observation that qAF was elevated in the melanin-free albino mice. Because the absence of pigment allows more light to be transmitted through the iris and through the eye wall posterior to the iris, one can expect intraocular light to be increased.^{47,48} It is also for this reason that subjects having lighter iris pigmentation have reduced contrast sensitivity and larger b-wave amplitudes at all illuminance levels.^{49,50} As demonstrated by increased intraocular light in the presence of hypopigmentation (carriers of *GPR143/OA1* mutations) or albinism (albino *Abca4*^{-/-}, C57BL/6J^{c2}), the SW-AF signal is modulated by variations in the levels of ocular pigment.

This study has clinical implications. The influence of ocular pigmentation on SW-AF intensities is important to an understanding of ethnicity-related differences in qAF values.²² A limitation of this study was that the cohort of *GPR143/OA1* carriers was relatively small. The difference in NIR-AF intensity in agouti- versus black-coated mice may call into question the assumption that RPE cell melanin content does not vary in concert with the melanin concentration in other tissues (e.g., iris, choroid, skin)^{6,51}; this will require further study. Nevertheless, NIR-AF imaging was shown to be of practical value for the identification of female *GPR143/OA1* carriers and affected patients. SW-AF imaging has become a part of standard care in retinal clinics, whereas NIR-AF imaging is rarely used. Nevertheless, the acquisition of NIR-AF images (HRA2; Heidelberg Engineering) is comfortable for patients because the NIR light is invisible. Diseased versus nondiseased areas of retina can be distinguished in NIR-AF images because of good contrast, and we found that a decline in NIR-AF can be predictive of ellipsoid zone loss in SD-OCT scans.¹² Thus efforts to understand the NIR-AF signal, as shown here, are important.

Acknowledgments

Supported by the National Eye Institute grants EY12951, EY024091, and P30EY019007, and a grant from Research to

Prevent Blindness to the Department of Ophthalmology, Columbia University.

Disclosure: **M. Paavo**, None; **J. Zhao**, None; **H.J. Kim**, None; **W. Lee**, None; **J. Zernant**, None; **C. Cai**, None; **R. Allikmets**, None; **S.H. Tsang**, None; **J.R. Sparrow**, None

References

- Delori FC, Dorey CK, Staurengi G, Arend O, Goger DG, Weiter JJ. In vivo fluorescence of the ocular fundus exhibits retinal pigment epithelium lipofuscin characteristics. *Invest Ophthalmol Vis Sci.* 1995;36:718-729.
- Sparrow JR, Gregory-Roberts E, Yamamoto K, et al. The bisretinoids of retinal pigment epithelium. *Prog Retin Eye Res.* 2012;31:121-135.
- Burke TR, Duncker T, Woods RL, et al. Quantitative fundus autofluorescence in recessive Stargardt disease. *Invest Ophthalmol Vis Sci.* 2014;55:2841-2852.
- Keilhauer CN, Delori FC. Near-infrared autofluorescence imaging of the fundus: visualization of ocular melanin. *Invest Ophthalmol Vis Sci.* 2006;47:3556-3564.
- Gibbs D, Cideciyan AV, Jacobson SG, Williams DS. Retinal pigment epithelium defects in humans and mice with mutations in MYO7A: imaging melanosome-specific autofluorescence. *Invest Ophthalmol Vis Sci.* 2009;50:4386-4393.
- Weiter JJ, Delori FC, Wing GL, Fitch KA. Retinal pigment epithelial lipofuscin and melanin and choroidal melanin in human eyes. *Invest Ophthalmol Vis Sci.* 1986;27:145-151.
- Duncker T, Tabacaru MR, Lee W, Tsang SH, Sparrow JR, Greenstein VC. Comparison of near-infrared and short-wavelength autofluorescence in retinitis pigmentosa. *Invest Ophthalmol Vis Sci.* 2013;54:585-591.
- Delori FC, Greenberg JP, Woods RL, et al. Quantitative measurements of autofluorescence with the scanning laser ophthalmoscope. *Invest Ophthalmol Vis Sci.* 2011;52:9379-9390.
- Cideciyan AV, Swider M, Aleman TS, Roman MI, Sumaroka A, Schwartz SB. Reduced-illumination autofluorescence imaging in ABCA4-associated retinal degenerations. *J Opt Soc Am A Opt Image Sci Vis.* 2007;24:1457-1467.
- Kellner U, Kellner S, Weinitz S. Fundus autofluorescence (488 nm) and near-infrared autofluorescence (787 nm) visualize different retinal pigment epithelium alterations in patients with age-related macular degeneration. *Retina.* 2010;30:6-15.
- Huang Z, Zeng H. Cutaneous melanin exhibiting fluorescence emission under near-infrared light excitation. *J Biomed Optics.* 2006;11:34010.
- Duncker T, Marsiglia M, Lee W, et al. Correlations amongst near-infrared and short-wavelength autofluorescence and spectral domain optical coherence tomography in recessive Stargardt disease. *Invest Ophthalmol Vis Sci.* 2014;55:8134-8143.
- Schuerch K, Marsiglia M, Lee W, Tsang SH, Sparrow JR. Multimodal imaging of disease-associated pigmentary changes in retinitis pigmentosa. *Retina.* 2016;36(Suppl 1):S147-S158.
- Kellner U, Kellner S, Weber BH, Fiebig B, Weinitz S, Ruether K. Lipofuscin- and melanin-related fundus autofluorescence visualize different retinal pigment epithelial alterations in patients with retinitis pigmentosa. *Eye (Lond).* 2009;23:1349-1359.
- Kellner S, Kellner U, Weber BH, Fiebig B, Weinitz S, Ruether K. Lipofuscin- and melanin-related fundus autofluorescence in patients with ABCA4-associated retinal dystrophies. *Am J Ophthalmol.* 2009;147:895-902.
- Duncker T, Lee W, Tsang SH, et al. Distinct characteristics of inferonasal fundus autofluorescence patterns in stargardt disease and retinitis pigmentosa. *Invest Ophthalmol Vis Sci.* 2013;54:6820-6826.
- Sparrow JR, Marsiglia M, Allikmets R, et al. Flecks in recessive Stargardt disease: short-wavelength autofluorescence, near-infrared autofluorescence, and optical coherence tomography. *Invest Ophthalmol Vis Sci.* 2015;56:5029-5039.
- Greenstein VC, Schuman AD, Lee W, et al. Near-infrared autofluorescence: its relationship to short-wavelength autofluorescence and optical coherence tomography in recessive Stargardt disease. *Invest Ophthalmol Vis Sci.* 2015;56:3226-3234.
- Duncker T, Greenberg JP, Sparrow JR, Smith RT, Quigley HA, Delori FC. Visualization of the optic fissure in short-wavelength autofluorescence images of the fundus. *Invest Ophthalmol Vis Sci.* 2012;53:6682-6686.
- Duncker T, Greenberg JP, Ramachandran R, et al. Quantitative fundus autofluorescence and optical coherence tomography in Best vitelliform macular dystrophy. *Invest Ophthalmol Vis Sci.* 2014;55:1471-1482.
- Duncker T, Tsang SH, Lee W, et al. Quantitative fundus autofluorescence distinguishes ABCA4-associated and non-ABCA4-associated bull's-eye maculopathy. *Ophthalmology.* 2015;122:345-355.
- Greenberg JP, Duncker T, Woods RL, Smith RT, Sparrow JR, Delori FC. Quantitative fundus autofluorescence in healthy eyes. *Invest Ophthalmol Vis Sci.* 2013;54:5684-5693.
- Early Treatment Diabetic Retinopathy Study Research Group. Early Treatment Diabetic Retinopathy Study design and baseline patient characteristics. ETDRS report number 7. *Ophthalmology.* 1991;98:741-756.
- Wu L, Nagasaki T, Sparrow JR. Photoreceptor cell degeneration in *Abcr*^{-/-} mice. *Adv Exp Med Biol.* 2010;664:533-539.
- Sparrow JR, Blonska A, Flynn E, et al. Quantitative fundus autofluorescence in mice: correlation with HPLC quantitation of RPE lipofuscin and measurement of retina outer nuclear layer thickness. *Invest Ophthalmol Vis Sci.* 2013;54:2812-2820.
- Ueda K, Zhao J, Kim HJ, Sparrow JR. Photodegradation of retinal bisretinoids in mouse models and implications for macular degeneration. *Proc Natl Acad Sci.* 2016;113:6904-6909.
- Khan KN, Lord EC, Arno G, et al. Detailed retinal imaging in carriers of ocular albinism. *Retina.* 2018;38:620-628.
- Sparrow JR, Blonska A, Flynn E, et al. Quantitative fundus autofluorescence in mice: correlation with HPLC quantitation of RPE lipofuscin and measurement of retina outer nuclear layer thickness. *Invest Ophthalmol Vis Sci.* 2013;54:2812-2820.
- Delori FC, Pflibsen KP. Spectral reflectance of the human ocular fundus. *Appl Optics.* 1989;28:1061-1077.
- Van Norren D, Tiemeijer LF. Spectral reflectance of the human eye. *Vision Res.* 1986;26:313-320.
- Wilk MA, Huckenpähler AL, Collery RF, Link BA, Carroll J. The effect of retinal melanin on optical coherence tomography images. *Trans Vis Sci Tech.* 2017;6(2):8.
- Mata NL, Weng J, Travis GH. Biosynthesis of a major lipofuscin fluorophore in mice and humans with ABCR-mediated retinal and macular degeneration. *Proc Natl Acad Sci U S A.* 2000;97:7154-7159.
- Kim SR, Fishkin N, Kong J, Nakanishi K, Allikmets R, Sparrow JR. The Rpe65 Leu450Met variant is associated with reduced levels of the RPE lipofuscin fluorophores A2E and iso-A2E. *Proc Natl Acad Sci U S A.* 2004;101:11668-11672.
- Maeda A, Golczak M, Maeda T, Palczewski K. Limited roles of Rdh8, Rdh12, and Abca4 in all-trans-retinal clearance in mouse retina. *Invest Ophthalmol Vis Sci.* 2009;50:5435-5443.

35. Flynn E, Ueda K, Auran E, Sullivan JM, Sparrow JR. Fundus autofluorescence and photoreceptor cell rosettes in mouse models. *Invest Ophthalmol Vis Sci.* 2014;55:5643-5652.
36. Cortese K, Giordano F, Surace EM, et al. The ocular albinism type 1 (OA1) gene controls melanosome maturation and size. *Invest Ophthalmol Vis Sci.* 2005;46:4358-4364.
37. Schiaffino MV. Signaling pathways in melanosome biogenesis and pathology. *Int J Biochem Cell Biol.* 2010;42:1094-1104.
38. Falletta P, Bagnato P, Bono M, et al. Melanosome-autonomous regulation of size and number: the OA1 receptor sustains PMEL expression. *Pigment Cell Melanoma Res.* 2014;27:565-579.
39. O'Donnell FE Jr, Hambrick GW Jr, Green WR, Iliff WJ, Stone DL. X-linked ocular albinism. An oculocutaneous macromelanosomal disorder. *Arch Ophthalmol.* 1976;94:1883-1892.
40. Riesz J, Gilmore J, Meredith P. Quantitative scattering of melanin solutions. *Biophys J.* 2006;90:4137-4144.
41. Poliakov E, Strunnikova NV, Jiang JK, et al. Multiple A2E treatments lead to melanization of rod outer segment-challenged ARPE-19 cells. *Mol Vis.* 2014;20:285-300.
42. Charbel Issa P, Barnard AR, Singh MS, et al. Fundus autofluorescence in the Abca4(-/-) mouse model of Stargardt disease—correlation with accumulation of A2E, retinal function, and histology. *Invest Ophthalmol Vis Sci.* 2013;54:5602-5612.
43. Tsai CL, Chen JC, Wang WJ. Near-infrared absorption property of biological soft tissue constituents. *J Med Biol Engineering.* 2001;21:7-14.
44. Rudolf M, Vogt SD, Curcio CA, et al. Histologic basis of variations in retinal pigment epithelium autofluorescence in eyes with geographic atrophy. *Ophthalmology.* 2013;120:821-828.
45. Fleckenstein M, Issa PC, Helb HM, et al. High-resolution spectral domain-OCT imaging in geographic atrophy associated with age-related macular degeneration. *Invest Ophthalmol Vis Sci.* 2008;49:4137-4144.
46. Song W, Zhang L, Ness S, Yi J. Wavelength-dependent optical properties of melanosomes in retinal pigmented epithelium and their changes with melanin bleaching: a numerical study. *Biomed Opt Express.* 2017;8:3966-3980.
47. van den Berg TJTP, Ijspeert JK, deWaard PWT. Dependence of intraocular straylight on pigmentation and light transmission through the ocular wall. *Vision Res.* 1991;31:1361-1367.
48. Coppens JE, Franssen L, van den Berg TJ. Wavelength dependence of intraocular straylight. *Exp Eye Res.* 2006;82:688-692.
49. Wali N, Leguire LE. Fundus pigmentation and the dark-adapted electroretinogram. *Doc Ophthalmol.* 1992;80:1-11.
50. Nischler C, Michael R, Wintersteller C, et al. Iris color and visual functions. *Graefes Arch Clin Exp Ophthalmol.* 2013;25:195-202.
51. Schmidt SY, Peisch RD. Melanin concentration in normal human retinal pigment epithelium. Regional variation and age-related reduction. *Invest Ophthalmol Vis Sci.* 1986;27:1063-1067.